Hovering Flight in the Honeybee Apis mellifera: Kinematic Mechanisms for Varying Aerodynamic Forces

Author(s): Jason T. Vance, Douglas L. Altshuler, William B. Dickson, Michael H. Dickinson and Stephen P. Roberts

Source: *Physiological and Biochemical Zoology: Ecological and Evolutionary Approaches*, Vol. 87, No. 6 (November/December 2014), pp. 870-881

Published by: The University of Chicago Press. Sponsored by the Division of Comparative Physiology and Biochemistry, Society for Integrative and Comparative Biology

Stable URL: https://www.jstor.org/stable/10.1086/678955

Hovering Flight in the Honeybee *Apis mellifera*: Kinematic Mechanisms for Varying Aerodynamic Forces

Jason T. Vance[1,*]
Douglas L. Altshuler[2]
William B. Dickson[3]
Michael H. Dickinson[4]
Stephen P. Roberts[5]
[1]Department of Biology, College of Charleston, Charleston, South Carolina 29424; [2]Department of Zoology, University of British Columbia, Vancouver, British Columbia V6T 1Z4, Canada; [3]IO Rodeo, Pasadena, California 91101; [4]Department of Biology, University of Washington, Seattle, Washington 98195; [5]Department of Biology, Central Michigan University, Mount Pleasant, Michigan 48859

Accepted 8/31/2014; Electronically Published 11/10/2014

Online enhancement: appendix figure.

ABSTRACT

During hovering flight, animals can increase the wing velocity and therefore the net aerodynamic force per stroke by increasing wingbeat frequency, wing stroke amplitude, or both. The magnitude and orientation of aerodynamic forces are also influenced by the geometric angle of attack, timing of wing rotation, wing contact, and pattern of deviation from the primary stroke plane. Most of the kinematic data available for flying animals are average values for wing stroke amplitude and wingbeat frequency because these features are relatively easy to measure, but it is frequently suggested that the more subtle and difficult-to-measure features of wing kinematics can explain variation in force production for different flight behaviors. Here, we test this hypothesis with multicamera high-speed recording and digitization of wing kinematics of honeybees (*Apis mellifera*) hovering and ascending in air and hovering in a hypodense gas (heliox: 21% O_2, 79% He). Bees employed low stroke amplitudes (86.7° ± 7.9°) and high wingbeat frequencies (226.8 ± 12.8 Hz) when hovering in air. When ascending in air or hovering in heliox, bees increased stroke amplitude by 30%–45%, which yielded a much higher wing tip velocity relative to that during simple hovering in air. Across the three flight conditions, there were no statistical differences in the amplitude of wing stroke deviation, minimum and stroke-averaged geometric angle of attack, maximum wing rotation velocity, or even wingbeat frequency. We employed a quasi-steady aerodynamic model to estimate the effects of wing tip velocity and geometric angle of attack on lift and drag. Lift forces were sensitive to variation in wing tip velocity, whereas drag was sensitive to both variation in wing tip velocity and angle of attack. Bees utilized kinematic patterns that did not maximize lift production but rather maintained lift-to-drag ratio. Thus, our data indicate that, at least for honeybees, the overall time course of wing angles is generally preserved and modulation of wing tip velocity is sufficient to perform a diverse set of vertical flight behaviors.

*Corresponding author; e-mail: vancejt@cofc.edu.

Physiological and Biochemical Zoology 87(6):870–881. 2014. 1522-2152/2014/8706-3090$15.00. DOI: 10.1086/678955

Introduction

Many flight-dependent behaviors of hovering animals require substantial aerodynamic reserves beyond those baseline requirements for stationary hovering flight. The high-frequency wingbeats that allow for sustained hovering also contribute to high maneuverability, rapid ascent, and load carriage in excess of body mass, such as during undertaking (transport and disposal of dead hive mates) in honeybees, blood feeding in mosquitoes, and prey carriage in cicada-hunting wasps. Studies of insects and hummingbirds filmed from single perspectives and at low sampling rates suggest that such aerodynamic reserves are realized at least in part by modulating wingbeat frequency (n) and wing stroke amplitude (Φ; Dudley 1995; Altshuler and Dudley 2003; Lehmann 2004; Roberts et al. 2004; Vance et al. 2009; Dillon and Dudley 2014). These gross kinematic parameters contribute to the angular and translational velocity of the wings (ω and U_t, respectively) and lift produced via delayed stall (Ellington 1984*b*; Dickinson et al. 1999; Sane and Dickinson 2002; Sane 2003). Other kinematic mechanisms are known to affect aerodynamic forces, such as angle of attack, the timing and velocity of wing rotation, and "clap and fling" (Sane 2003); however, these mechanisms have not been observed in insects as a strategy to augment aerodynamic output during simple, bilaterally symmetric flight behaviors, such as ascending or hovering in hypodense atmospheres.

Aerodynamic forces scale in proportion to the square of wing velocity, and hovering species modulate wingbeat frequency and/or stroke amplitude to increase angular and translational velocity and increase forces during hovering flight. For example, hummingbirds (*Archilochus colubris*) and carpenter bees (*Xylocopa varipuncta*) increase both stroke amplitude and wingbeat frequency during load lifting or maximal

hovering flight in hypodense gas (Chai and Dudley 1996; Chai 1997; Altshuler and Dudley 2003; Roberts et al. 2004). Orchid bees (Apidae: Euglossini) hold wingbeat frequency constant but increase stroke amplitude by 30%–45% during maximal hovering flight in hypodense gas (Dudley 1995). During tethered flight, fruit flies (*Drosophila melanogaster*) increase total flight force by increasing both stroke amplitude and wingbeat frequency; however, as *Drosophila* approach their ceiling of muscle power output, further increases in stroke amplitude and wing tip velocity are accomplished only with a concomitant decrease in stroke frequency (Lehmann and Dickinson 1997). Mature honeybees (*Apis mellifera*) of the foraging caste, like orchid bees, maintain wingbeat frequency while increasing stroke amplitude during maximal hovering flight in hypodense gas (Vance et al. 2009). However, like *Drosophila* (Lehmann and Dickinson 1997), immature bees and very old honeybees are unable to maintain wingbeat frequency while increasing stroke amplitude, which ultimately impairs their maximal hovering capacity (Vance et al. 2009).

Beyond modulating stroke amplitude and wingbeat frequency, insects possess a broad suite of kinematic mechanisms to vary aerodynamic force production, several of which are observed during turning maneuvers. For example, fruit flies use transient, bilateral asymmetries in stroke amplitude, stroke plane angle (Fry et al. 2003), and angle of attack (Ristoph et al. 2010) to perform yaw turns (saccades) and correct for yaw-axis perturbations during free flight. Dragonflies also vary wing angle of attack to perform more complex roll and yaw turns (Alexander 1986). Dynamically scaled modeling has further demonstrated that the timing and velocity of wing rotation during the stroke reversal affect rotational lift production (Sane 2003). These aerodynamic mechanisms are interesting for the case of honeybees, which rely on significant wing rotation and wing wake interactions during hovering flight (Altshuler et al. 2005). If present, variation in wing rotation would provide insight into how some bees are able to augment aerodynamic force to accommodate moderate pollen loads while holding stroke amplitude and wingbeat frequency constant (Feuerbacher et al. 2003). Aerodynamic force production may also benefit from clap and fling, where wing contact and the following stroke reversal promote the formation of a leading-edge vortex early in the wing stroke (Ellington 1999; Lehmann et al. 2005). Clap and fling is observed in a variety of fliers and has been successfully leveraged by flapping-wing microaerial vehicles (Zdunich et al. 2007); however, the use of clap and fling as a transient mechanism to augment lift on demand has not been well characterized in insects.

Although aerodynamic forces may be affected by several kinematic strategies, it is unknown whether honeybees or other insects vary multiple kinematic parameters besides wingbeat frequency and stroke amplitude to augment lift during hovering and ascending flight. The purpose of this study was to investigate the kinematics used by honeybees under the aerodynamic challenges of ascending flight in air and hovering flight in hypodense atmospheres as compared to hovering flight in air. We were particularly interested in whether varying angle of attack made a substantial contribution similar to that of modulating wing tip velocity. This was accomplished using three-dimensional high-speed video analysis of bees hovering and ascending in normal air and hovering in hypodense heliox gas. Using stereotyped honeybee hovering kinematics (Altshuler et al. 2005), we employed a quasi-steady aerodynamic model to examine the aerodynamic consequences of varying wing tip velocity and angle of attack across a range that overlapped with the observed kinematics. These results were then compared to the aerodynamic forces estimated from the observed kinematics of individual bees to evaluate whether bees augment aerodynamic output using kinematic strategies that favor optimal lift production or economize between the production of lift and drag.

Material and Methods

Collection and Filming of Bees

European honeybees (*Apis mellifera*) were collected as they exited a hive at the University of Nevada–Las Vegas campus apiary and were immediately transferred to an 8-L transparent acrylic flight chamber in an adjacent laboratory. The temperature in the flight chamber was held constant at 30°C for all measurements. A sucrose solution and pollen grains were placed on a pedestal centrally located within the flight chamber, which provided the honeybees with sustenance and created a focal target for video recording. Three high-speed video cameras, oriented orthogonally to each other, recorded honeybee flight at either 6,000 frames per second (Photron Ultima APX, San Diego, CA; 512 × 512 pixel resolution) or 6,006 frames per second (Vision Research Phantom v5.1, Wayne, NJ; 400 × 400 pixel resolution). One to three bees occupied the flight chamber during any given collection run, but only one bee was in flight during any recorded trial. Bees were monitored until an acceptable flight sequence (e.g., a bee in focus in all three cameras) was recorded, the bees demonstrated lethargy, and/or 30 min elapsed.

Flight Conditions

To assess how bees modulate kinematics and aerodynamic force production during simple vertical modes of flight, we filmed bees during hovering ($N = 5$; mass $= 115.9 \pm 29.6$ mg) and ascending ($N = 9$; 120.4 ± 21.2 mg) flight in normal air and during hovering in pure heliox ($N = 4$; 119.8 ± 31.0 mg). Normoxic heliox (21% O_2/79% He) has a low air density (0.41 kg m^{-3}), one-third that of normal air (21% O_2/79% N_2; 1.21 kg m^{-3}). Hovering in heliox requires the same vertical force as hovering in air but requires greater sustained power output from the flight muscles (Dudley 1995), whereas ascending flight requires greater vertical force during acceleration and greater power than hovering. The heliox was mixed using calibrated bimetal thermoactuated valves (Tylan FC-460; San Diego, CA), metered by an electronic flow controller

(Sable Systems MFC-4; Las Vegas, NV), and maintained at a total flow rate of 1 L min^{-1} throughout the trial.

Video Processing and Kinematic Analysis

Digital video recordings were processed and analyzed using methods described by Altshuler et al. (2005). Flight sequences were analyzed as individual bitmap images using custom software (Fry et al. 2003) written in Matlab (Mathworks, Natick, MA). Prior to the analysis of each trial, the focal volume was calibrated using anatomical landmarks on the bee that were visible from all three cameras. The kinematic analysis of each trial utilized six landmarks that were digitized using at least two camera views (fig. 1): head, tip of abdomen, left and right wing hinges, and left and right wing tips. To determine the geometric angle of attack (α), we superimposed a wire frame wing image over the bee wing in all camera views and rotated the wire frame about the long axis (wing hinge to wing tip) until optimal overlap was achieved, emphasizing the distal half of the wing, where translational velocity is highest. A cubic spline was used to smooth the landmark position data, followed by a frame-by-frame verification of adherence to the video record. From these landmarks, we determined the time histories of the following kinematic variables (as defined by Ellington 1984*a*) during each frame of the recorded flight sequence: body angle (χ), wing position angle (ϕ) within the stroke plane, wing deviation angle (θ) from the stroke plane, translational velocity of the wing tip (U_t; calculated from ϕ, θ, and R), geometric angle of attack (α), and wing rotational velocity ($\dot{\alpha}$; calculated as rate of change of α). The following kinematic variables were calculated across individual wing strokes: absolute stroke plane (β), body-relative stroke plane angle (β_r), and wingbeat frequency (n). Ten to 14 complete wingbeat cycles from each bee were analyzed to determined minimum, maximum, or stroke-averaged values for these kinematic parameters. Advance ratio and vertical velocity were used to characterize hovering and ascending flight behaviors. Advance ratio was calculated as the quotient of average velocity and average wing tip velocity. Average vertical velocity was determined from the quotient of vertical displacement and duration of the flight sequence. Calculations of vertical acceleration were made difficult by the very low time increment resulting from the high-speed video record and short duration of the flight sequences. Efforts to filter, decimate, or curve fit the position data did not produce reliable vertical acceleration estimates; thus, we do not present these data.

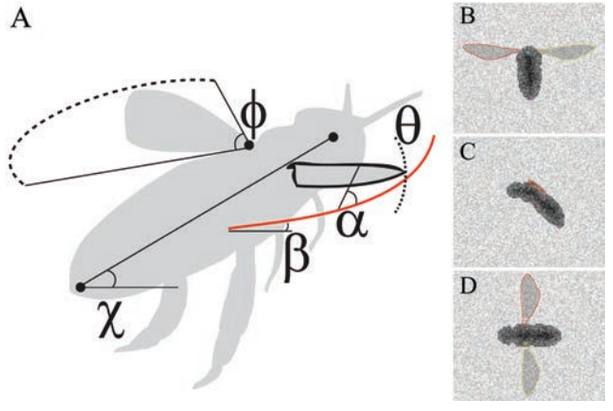

Figure 1. *A*, Body landmarks (head, abdomen, wing hinges, and wing tips) used to calculate flight kinematics: body angle (χ), wing position angle (ϕ) within the stroke plane (dashed line), wing deviation angle (θ; dotted line) from the stroke plane (red line), geometric angle of attack (α), and absolute stroke plane (β). Body landmarks were digitized from front (*B*), side (*C*), and top (*D*) camera views; the bee is facing the reader in the front (*B*) camera view. Right (red) and left (yellow) wing wire frames are superimposed over the wings to determine geometric angle of attack. The methods illustrated in *B–D* depict the three-dimensional model honeybee that was used to calculate digitizing error (see app. A).

Aerodynamic Analysis

Our previous research employed dynamically scaled and quasi-steady aerodynamic models to determine how varying stroke amplitude and wing tip velocity affected aerodynamic force production (Altshuler et al. 2005); however, we did not investigate whether honeybees modulate geometric angle of attack or how such strategies might affect aerodynamic forces. To compare the aerodynamic consequences of varying stroke amplitude and geometric angle of attack, we created a series of artificial time histories for wing position angle (ϕ), wing deviation angle (θ), and geometric angle of attack (α), based on the kinematic patterns extracted from the three flight conditions described above. The kinematic time histories of wing tip velocity were scaled such that stroke amplitude ranged from 70° to 170° (fig. 2*A*) at a fixed wingbeat frequency (n = 220 Hz), which adequately spanned the range of wing tip velocity observed in this study and is representative of the range in stroke amplitude observed in several bee species (Dudley 1995; Roberts et al. 2004; Vance et al. 2009), including the bees in this study (Φ = 79°:152°). The time histories of geometric angle of attack were scaled such that the stroke-averaged geometric angle of attack ranged from 40° to 65° (fig. 2*A*), significantly beyond the range of stroke-averaged geometric angle of attack we observed, to determine whether bees capitalized on optimal patterns of wing rotation. The time course of wing stroke deviation was constant across trials, thus limiting our analysis to variation in wing tip velocity (via stroke amplitude) and geometric angle of attack. Using these modeled kinematics, wing parameters, and steady state lift and drag coefficients (C_L and C_D, respectively; fig. 2*B*) from Altshuler et al. (2005), we estimated translational lift (L) and drag (D) forces via a quasi-steady model (Sane and Dickinson 2002):

$$L(t) = \frac{1}{2}\rho\, S|U_t(t)|^2\, \hat{r}_2^2 C_L[\alpha_{aero}(t)],$$

$$D(t) = \frac{1}{2}\rho\, S|U_t(t)|^2\, \hat{r}_2^2 C_D[\alpha_{aero}(t)],$$

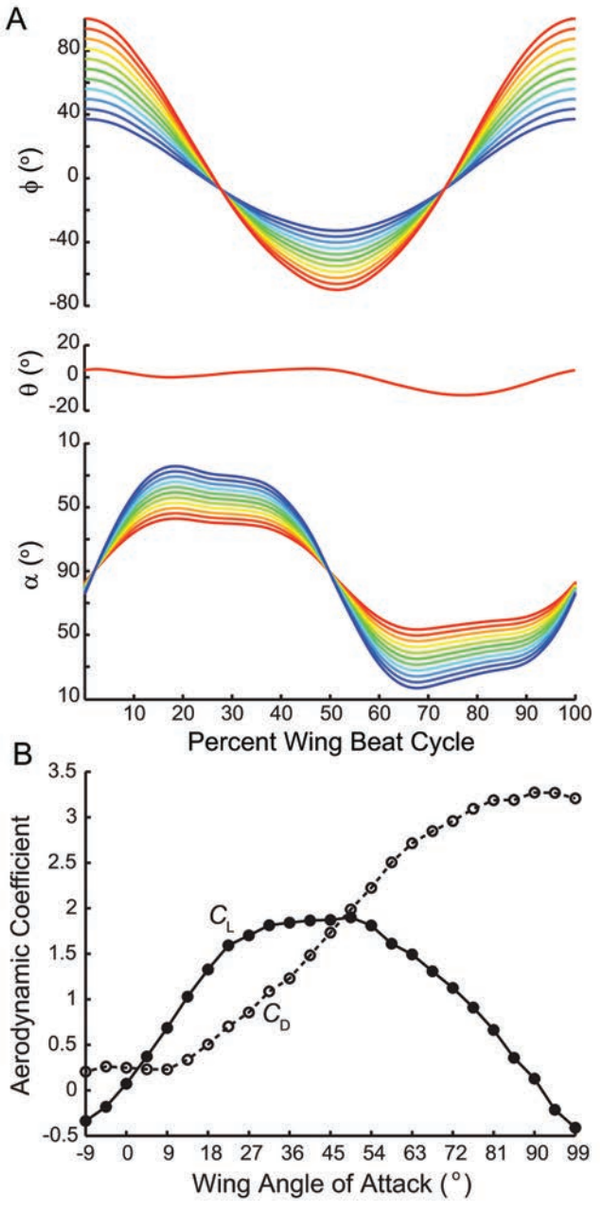

Figure 2. *A*, Artificial kinematics used for the aerodynamic model were created by scaling the time history of wing stroke position (ϕ) and geometric angle of attack (α). The time history of wing stroke deviation (θ) was maintained. *B*, Aerodynamic coefficients of lift (C_L; filled circles) and drag (C_D; open circles), as a function of angle of attack, were calculated from measurements of a model of the honeybee wing revolving at a fixed velocity in mineral oil at Re 970 (Altshuler et al. 2005). Figure published in Vance et al. (2013).

where gas density, ρ, represented the density of air for all conditions; wing area, S (52.7 mm^2), and second moment of area, r_2^2 (0.555), were calculated from morphological measurements averaged across the bees tested; and aerodynamic angle of attack, α_{aero}, was calculated from the geometric angle of attack and the vector of wing translation, determined by wing stroke position and wing deviation angle. We then estimated the translational forces resulting from each bee's actual kinematics to evaluate where individual kinematic strategies fell along the continuum of wing tip velocity and stroke-averaged geometric angle of attack tested in our model, as described above. We were specifically interested in whether bees' kinematic strategies reveal any prioritization toward maximizing lift at the expense of drag or maximizing the ratio of lift to drag when modulating aerodynamic forces. Stroke-averaged aerodynamic forces were calculated from the instantaneous aerodynamic forces during the course of each wing stroke and were reported for both the aerodynamic model and the individual bee force estimates.

Results

While hovering in air and heliox, honeybees maintained a vertical velocity less than 1 cm s^{-1}, whereas bees filmed during ascension moved upward at approximately 33 cm s^{-1}, averaged across the duration of the flight sequence. Although we were unable to reliably calculate acceleration over the short distance of each flight sequence, ascending bees would require appreciable acceleration to achieve such high average velocities over the short vertical distance available within the flight chamber. The kinematics of honeybee hovering and ascending flight are characterized by high-frequency wing strokes ($n = 228.6 \pm 17.8$ Hz) that are dorsally biased with respect to the wing hinges (fig. 3). Simple hovering flight in air was accomplished with low stroke amplitude, Φ (86.7° $\pm$ 7.9°), which increased by 30% during ascending flight and by 47% during hovering flight in heliox. These changes resulted from increases in both dorsal and ventral excursion (table 1; figs. 3, 4). The wingbeat frequency did not vary among conditions (table 2). Bees employed a planar downstroke that is nearly horizontal and a U-shaped upstroke (fig. 5). Although the amplitude of the deviation from the stroke plane, Θ, was greater during the upstroke than the downstroke, there were no differences across the three flight conditions. Geometric angle of attack averaged across the wing stroke (α_{avg}) was greater during the upstroke than the downstroke for all bees (table 3). However, again there were no significant differences in the stroke-averaged or minimum geometric angle of attack (which occurs near midstroke) across the three flight conditions. Maximum wing rotation velocity, near the stroke reversal, was greater in magnitude and delayed in phase at the end of the upstroke as compared to the end of the downstroke; however, there were no differences in wing rotation velocity or phase across the three flight conditions (table 3). There were also no significant differences in body angle (χ) or absolute and body-relative stroke plane angles (β and β_r, respectively) across the three conditions (table 2). Although three of the four bees hovering in heliox exhibited 55% greater body angle than bees hovering in air, one bee hovered with a very shallow body angle (28°), which contributed to the high standard deviation and nonsignificant trend in the heliox group.

Ascending in normal air and hovering in pure heliox require greater aerodynamic power output compared to hov-

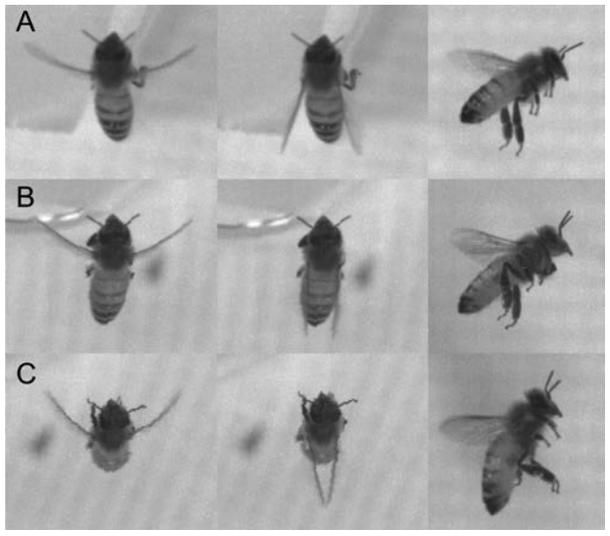

Figure 3. Honeybees during hovering in air (*A*), ascending in air (*B*), and hovering in heliox (*C*). Columns (from left to right) depict ventral stroke reversal, dorsal stroke reversal, and body angle.

ering in normal air. However, despite the increased challenges, the bees maintained the same body angle, stroke plane angle, deviation, geometric angle of attack, and wingbeat frequency across the three conditions. Thus, the only measured mechanism that they employed was modulation of the stroke amplitude, which in turn caused changes in wing tip velocity, U_t (fig. 4; table 3), a critical feature for aerodynamic force and power. During ascending flight, wing tip velocity was 26% greater during the downstroke (air: $U_{t,down} = 10.5 \pm 1.0$ m s^{-1}; ascending: $U_{t,down} = 13.2 \pm 1.6$ m s^{-1}) and 23% greater during the upstroke (air: $U_{t,up} = 10.8 \pm 1.5$ m s^{-1}; ascending: $U_{t,up} = 13.3 \pm 1.9$ m s^{-1}) than bees hovering in air. Likewise, during hovering in heliox, wing tip velocity was 47% greater during the downstroke ($U_{t,down} = 15.4 \pm 2.7$ m s^{-1}) and 46% greater during the upstroke ($U_{t,up} = 15.8 \pm 2.5$ m s^{-1}) than during hovering in air.

In our aerodynamic model using the stereotyped kinematics (fig. 2), stroke-averaged lift forces increased from 0.948×10^{-3} to 3.905×10^{-3} N across a range in wing tip velocity equivalent to that which would result from a 100° increase in stroke amplitude ($\Phi = 70°:170°$) with constant wingbeat frequency (fig. 6*A*). Variation in the time course of geometric angle of attack had a minor effect on lift, with maximum lift production resulting from a narrow range in stroke-average geometric angle of attack, ranging from 54.5° to 56° across wing tip velocity. As can be seen in the surface plot of figure 6*B*, independently increasing just wing tip velocity at low angles of attack or increasing geometric angle of attack at low wing tip velocities produced only moderate effects on drag forces (fig. 6*B*). However, the combination of increasing both wing tip velocity and geometric angle of attack had a substantial influence on drag force. Based on this relationship, lift-to-drag ratio ($L:D$) has a strong, inversely proportional relationship to geometric angle of attack. At shallow geometric angles of attack,

Table 1: Kinematic values during hovering and ascending in air and hovering in heliox

	Hovering (5)	Ascending (9)	Heliox (4)
n (Hz)	226.8 ± 12.8	218.3 ± 24.0	238.6 ± 11.4
Φ (°)	86.7 ± 7.9	115.0 ± 14.3	127.5 ± 25.6
ϕ_{mean} (°)	36.4 ± 2.8	41.8 ± 3.4	45.2 ± 6.1
Θ (°)	11.8 ± 6.7	9.5 ± 4.8	10.6 ± 5.9
α_{min} (°)	25.3 ± 6.2	27.0 ± 4.4	26.5 ± 4.3
α_{avg} (°)	46.1 ± .5	45.1 ± 2.8	45.0 ± 2.7
U_t (m s^{-1})	10.7 ± 1.2	13.2 ± 1.7	15.6 ± 2.4
$\dot{\alpha}$ (rad s^{-1})	2,555 ± 157	2,502 ± 387	2,673 ± 295
Phase (°)	1.5 ± 2.2	.8 ± 2.2	.1 ± 2.1
χ (°)	39.6 ± 3.7	44.8 ± 5.4	53.3 ± 19.0
β (°)	−3.4 ± 4.9	−.8 ± 3.1	2.7 ± 9.2
β_r (°)	44.5 ± 2.8	46.0 ± 5.3	50.4 ± 10.9
Re	1,163 ± 98	1,477 ± 159	1,793 ± 298
V_{vert} (m s^{-1})	.005 ± .042	.328 ± .141	.009 ± .087
AR	.030 ± .010	.050 ± .016	.018 ± .012
L (10^{-3} N)	1.41 ± .25	2.18 ± .49	3.27 ± 1.00
D (10^{-3} N)	1.11 ± .18	1.66 ± .34	2.51 ± .64
$L:D$	1.27 ± .08	1.31 ± .10	1.29 ± .14

Note. Kinematic units are shown in parentheses after each parameter. Sample sizes for hovering and ascending in air and hovering in heliox are shown in parentheses after each state. The Reynolds number (Re), advance ratio (AR), and lift-to-drag ratio ($L:D$) are dimensionless. Values were calculated by taking the treatment means ± SD from individual means. See table A1 for definitions of symbols.

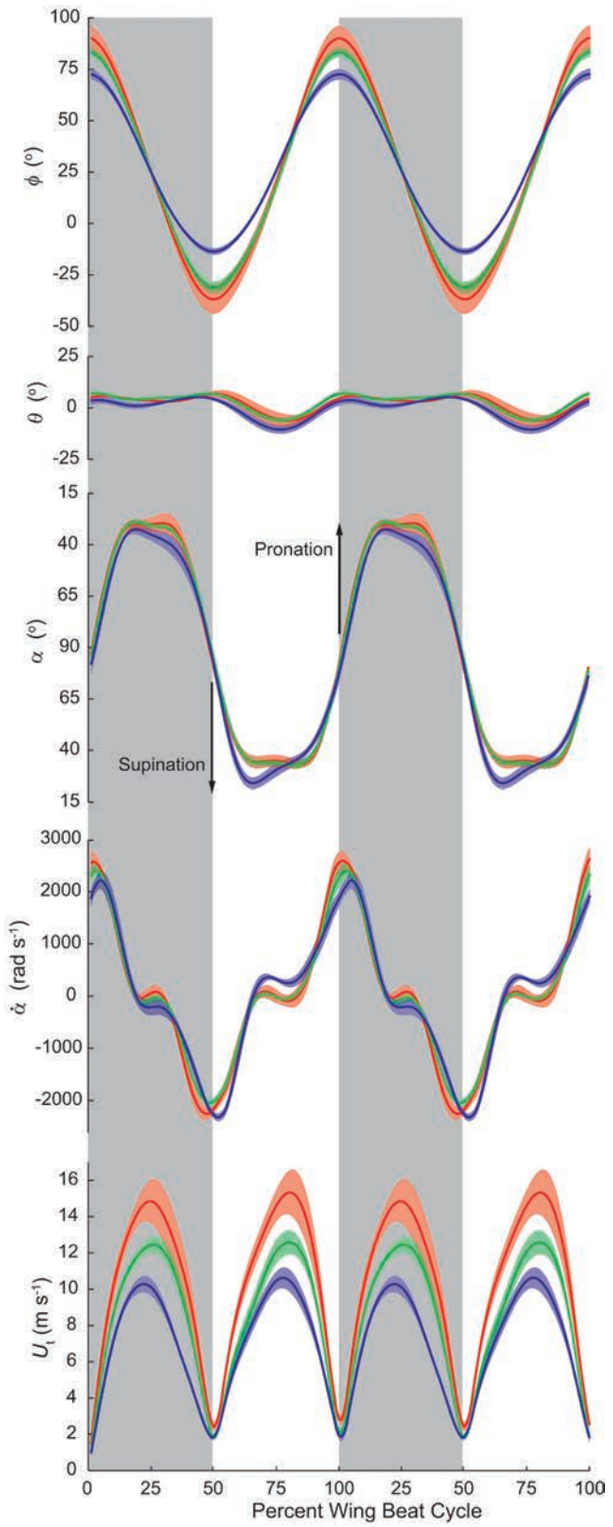

Figure 4. Mean kinematic patterns of wing stroke position (ϕ), deviation from the mean stroke plane (θ), geometric angle of attack (α), wing rotation velocity (α), and wing tip velocity (U_t) during hovering in air (blue), ascending in air (green), and hovering in heliox (red). The time course of the kinematic patterns is normalized to 100% of the wingbeat cycle and averaged across all wingbeats per bee, per group. The shaded regions indicate ±SE about the mean kinematic pattern (solid line). The gray and white columns indicate the downstrokes and upstrokes, respectively.

$L:D$ is high and gradually increases with wing tip velocity. This observation seems counterintuitive, as wing tip velocity is a parameter shared by the calculations for both lift and drag. However, because the time course of wing stroke deviation does not vary in our aerodynamic model, variation in wing tip velocity—via stroke amplitude—influences the wing tip trajectory (see fig. 5, lateral view) and resulting aerodynamic angle of attack for any given geometric angle of attack. As geometric angle of attack increases, variation in wing tip velocity, and its subtle influence on the wing tip trajectory and resulting aerodynamic angle of attack, has less effect on $L:D$.

For forces estimated from individual bees, lift and drag predominately increased with wing tip velocity, as stroke-averaged geometric angle of attack varied across only a narrow range. Forces estimated by the model during ascending flight were greater than during hovering in air (table 2); however, $L:D$ was conserved between these two conditions. Forces estimated from the kinematics used during hovering in heliox reflect the density of air rather than heliox and were excluded from the statistical analysis of aerodynamic variables (i.e., Reynolds number [Re], lift, drag, and $L:D$). However, we included these data in table 1 and figure 6 to illustrate the extent by which kinematics variation observed across the three flight conditions might augment aerodynamic force. The increased stroke amplitude and wing tip velocity observed during flight in heliox produced the greatest lift and drag forces using our aerodynamic model, yet $L:D$ was comparable to hovering and ascending in air.

Discussion

To meet the aerodynamic demands of ascending flight in air and hovering in heliox, honeybees modulate wing tip velocity by increasing stroke amplitude while maintaining wingbeat frequency. Based on other studies of insect flight kinematics, we sought to determine whether bees modulated other kinematic parameters, such as wing geometric angle of attack, rotation velocity, and deviation. Within all flight conditions there were considerable differences in kinematic variables between the downstroke and the upstroke. Specifically, stroke deviation was greater during the upstroke than the downstroke, whereas stroke-averaged geometric angle of attack was greater during the downstroke than the upstroke. Peak wing rotation velocity was greater during the dorsal stroke reversal—and its phase was delayed to the dorsal stroke reversal—than during the ventral stroke reversal, where its phase was advanced. However, none of these stroke-specific variables differed across the three flight conditions. Nonetheless, we

Table 2: Results of one-way ANOVA for kinematic and aerodynamic variables

	Flight condition	
	F	P
n	1.54	.247
Φ	8.10	.004[a]
ϕ_{mean}	5.73	.014[b]
χ	2.31	.133
β	1.45	.265
β_r	.99	.395
Re	15.9	.002
V_{vert}	18.46	<.001[c]
AR	8.66	.003[c]
L	10.6	.007
D	11.5	.005
$L:D$	.53	.480

Note. One-way ANOVA ($F_{1,17}$) for all kinematic variables during hovering and ascending in air and hovering in heliox. One-way ANOVA for aerodynamic variables (L, D, $L:D$, and Re) during hovering and ascending in air ($F_{1,13}$). Significant differences are indicated by P value < 0.05. Units are provided in table 1 and definitions of symbols in table A1.

[a]Tukey's HSD: ascending and heliox > hovering.

[b]Tukey's HSD: heliox > hovering.

[c]Tukey's HSD: ascending > hovering and heliox.

observed variation in the time course of geometric angle of attack and deviation angle (fig. 4) that could potentially impact instantaneous and stroke-averaged lift and drag forces. For the quasi-steady aerodynamic model, lift forces increased considerably with wing tip velocity but did not vary with geometric angle of attack across the range of values considered (fig. 6). Drag forces increased with both geometric angle of attack and wing tip velocity. $L:D$ was greatly influenced by geometric angle of attack but relatively invariant across wing tip velocity. Because the honeybees maintained similar angles of attack among individuals and across flight treatments, $L:D$ estimated by our model was conserved. These results suggest that for vertical flight performance, even though other kinematic strategies may augment lift at the expense of drag, bees manipulate a reduced set of kinematic parameters that economizes their $L:D$.

Several bee species, including honeybees, vary wingbeat frequency as an apparent thermoregulatory mechanism (Unwin and Corbet 1984; Spangler and Buchmann 1991; Harrison et al. 1996; Roberts and Harrison 1998; Borrell and Medeiros 2004); however, some Anthophorine species, such as *Xylocopa varipuncta* and *Centris pallida*, modulate frequency to control aerodynamic power output (Roberts et al. 2004; Roberts 2005). Despite their ability to increase wingbeat frequency inversely proportional to ambient temperature, the honeybees in this study, like their *Bombus* and *Euglossine* relatives (Dudley 1995; Dillon and Dudley 2014), did not vary frequency as a mechanism to modulate lift production. Bumblebees and honeybees employ wingbeat frequencies that are extraordinarily high for their body mass and wing size (Greenewalt 1962), and honeybees in particular may be constrained by the mass and stiffness of their thoracic morphology, wings, and flight muscle to operate near their resonant frequency. For example, when the wing area of mature foragers is experimentally reduced, they have lower wing mass and increase their wingbeat frequency (Vance 2009). Conversely, immature honeybee foragers and nurses are able to fly in normal air but, compared to mature foragers, fail at higher gas densities when challenged to fly in hypodense atmospheres due to their inability to maintain wingbeat frequency (Vance et al. 2009). Their decreased flight performance is presumably due to the biochemical development of the flight muscle (Schippers et al. 2006) and reduced muscle force (Marden et al. 2001) and stiffness. These results suggest that honeybee flight muscle has a narrow operating range of wingbeat frequency that is presumably tuned about the resonant properties of the flight motor. Furthermore, augmenting aerodynamic power output via an increase in both wingbeat frequency and stroke amplitude would require greater inertial power than increasing stroke amplitude alone (Ellington 1984*c*). Thus, modulating stroke amplitude while employing wing angles of attack that maintain high $L:D$ may provide economy during the long-distance load carriage required for foraging behavior to offset the metabolic expenditure of otherwise maintaining such high operating frequencies.

Simple hovering flight requires high mass-specific metabolic rates (Withers 1981; Coelho and Mitton 1988; Harrison 1986; Suarez et al. 1996, 2005; Roberts et al. 2004), yet hovering animals possess significant aerodynamic reserves to allow for load carriage, accommodating atmospheric pertur-

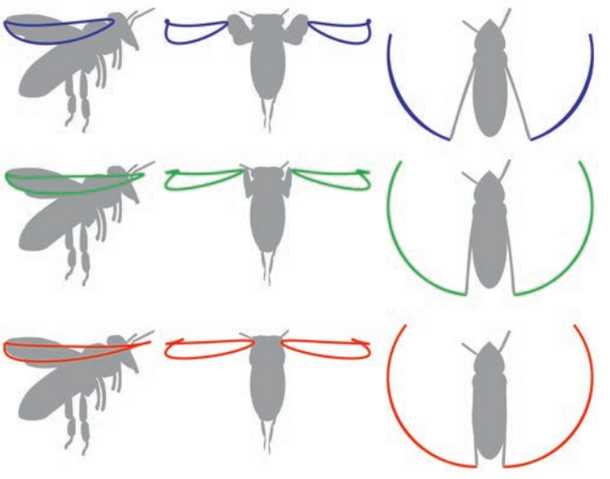

Figure 5. Lateral, dorsal, and top views (left, middle, and right columns, respectively) of mean wing tip trajectories, composed from wing stroke position and deviation from the mean stroke plane and averaged across all wingbeats per bee during hovering in air (blue), ascending in air (green), and hovering in heliox (red). Bees employ relatively planar, horizontal downstrokes and U-shaped upstrokes. Although there was a tendency for amplitude of deviation from the stroke plane to decrease as wing stroke amplitude increased, this trend was not significant.

Table 3: Results of two-way ANOVA for kinematic variables

	Flight condition		Stroke	
	F	*P*	*F*	*P*
Θ	2.35	.111	110.2	<.001
α_{min}	.35	.708	.07	.796
α_{avg}	.16	.856	19.4	<.001
$\dot{\alpha}$	1.00	.378	10.1	.003
U_t	16.8	<.001[a]	.10	.757
Phase	1.39	.265	16.54	<.001

Note. Two-way ANOVA for kinematic variables during hovering and ascending in air and hovering in heliox (flight condition; $F_{2,35}$) and during the wing downstroke and upstroke (stroke; $F_{1,35}$). Significant differences are indicated by P value < 0.05. Units are provided in table 1 and definitions of symbols in table A1. There were no significant flight condition × stroke interactions.

[a]Tukey's HSD: heliox > ascending > hovering.

bations and maneuvering. During hovering in heliox, honeybees increased stroke amplitude by 47% (figs. 3, 4), similar to other bee species, including *X. varipuncta* (Roberts et al. 2004) and *Euglossine* spp. (Dudley 1995). The range of motion of bees' wing strokes is biased dorsally to the wing hinges, and honeybees increased stroke amplitude through a disproportionate increase in dorsal excursion. The thorax and wing hinge morphologies, which are generally similar across bee species, appear to limit ventral wing excursion. As the mean stroke position rotates further dorsally with increases in stroke amplitude, the resulting aerodynamic center of pressure also shifts dorsally. The ability to generate a moment about the pitch axis should increase under these conditions, which would be conducive to maintaining body angle with increased foraging load.

Dorsal excursion in the wing stroke was ultimately limited by wing contact at the dorsal stroke reversal, which was observed in several bees during hovering in heliox (fig. 3). These extreme dorsal stroke kinematics appear similar to those that produce aerodynamic force via clap and fling. In application, the clap forces air out from between the area where the two wings are in contact, and the fling causes air to rush over the leading edges as the wings peel apart, enhancing the development of vorticity early in the downstroke when wing tip velocity is low (Ellington 1999; Lehmann et al. 2005). This aerodynamic mechanism is utilized by a variety of insects, ranging from small parasitic wasps (Miller and Peskin 2005) to damselflies (Wakeling and Ellington 1997*a*, 1997*b*), and has been successfully exploited at much larger scales in micro-aerial vehicle (MAV) development, such as the *Mentor* MAV (Zdunich 2007). However, the degree to which a clap-and-fling kinematic pattern increases lift is crucially dependent on the precise kinematics of the wing (Lehmann et al. 2005; Lehmann and Pick 2007), and its mere presence does not necessarily indicate a substantial augmentation in force. Nonetheless, whether clap and fling is employed as a lift-enhancing mechanism, bees' ability to vary stroke amplitude across such a large range facilitates substantial aerodynamic reserves that allow bees to meet the demands of their various flight behaviors.

Individual variation in the time course and magnitude of geometric angle of attack has the potential to affect lift and drag forces. Bees displayed minimum angles of attack, near midstroke, that ranged from 21.7° to 33.8° and stroke-averaged angles of attack that ranged from 41.1° to 50.5°. To evaluate how variation in geometric angle of attack impacted aerodynamic forces, we scaled the artificial kinematics over a range of stroke-averaged angles of attack (40°–65°; fig. 2*A*) greater than that observed in these bees. Lift and drag coefficients relative to wing geometric angle of attack were determined using a physical model of the bee wing during a previous experiment (fig. 2*B*; adapted from fig. 4 of Altshuler et al. 2005). The lift and drag coefficients reveal two patterns of particular relevance to the current theoretical model: (1) the range of geometric angle of attack under consideration is inclusive of the region (49.5°) with the maximum lift coefficient and (2) the lift coefficient varies relatively little across a broad range of geometric angle of attack (22.5°–63°), whereas drag coefficient varies considerably. As a result, aerodynamic lift forces were generally insensitive to variation in the geometric angle of attack tested in our model, especially when compared to the marked effect of wing tip velocity (fig. 6*A*). Conversely, drag forces are highly sensitive to variation in geometric angle of attack across wing tip velocity (fig. 6). Therefore, increasing stroke-averaged geometric angle of attack, up to approximately 55°, would produce only modest gains in lift while generating significantly greater drag. Honeybees utilized stroke-averaged angles of attack approximately 10° less than where maximum lift was estimated in the theoretical model. This suggests that bees do not change their pattern of geometric angle of attack to maximize lift, at the expense of drag, when ascending in air or hovering in heliox. Rather, bees employed a pattern of geometric angle of attack that preserved $L:D$ while instead modulating wing tip velocity to meet the aerodynamic demands of the three flight conditions. The plateau in the coefficient of lift profile (fig. 2*B*) is not unique to honeybees, but it also seen in fruit flies (Dickinson and Gotz 1993; Dickinson 1994), dragonflies (Kesel 2000), bumblebees (Dudley and Ellington 1990), hawkmoths (Usherwood and Ellington 2002), and hummingbirds (Altshuler et al. 2004). Thus, hovering animals operating at or near maximum coefficient of lift might also benefit from varying wing tip velocity to modulate vertical force production and instead vary geometric angle of attack during modes of flight where modulating drag forces are important, such as for producing thrust (Ristroph et al. 2011) or generating yaw-axis body moments (Ristroph et al. 2010; Vance et al. 2013). Engineered solutions for MAVs have further leveraged the modulation of wing tip velocity to reduce longitudinal and lateral flight control to a single degree of freedom about each wing (Ma et al. 2013).

We did not observe any bees manipulating geometric angle of attack in a manner that might explain the paradoxical results of Feuerbacher et al. (2003), in which honeybees accommodated pollen loads that equaled 18% of body mass

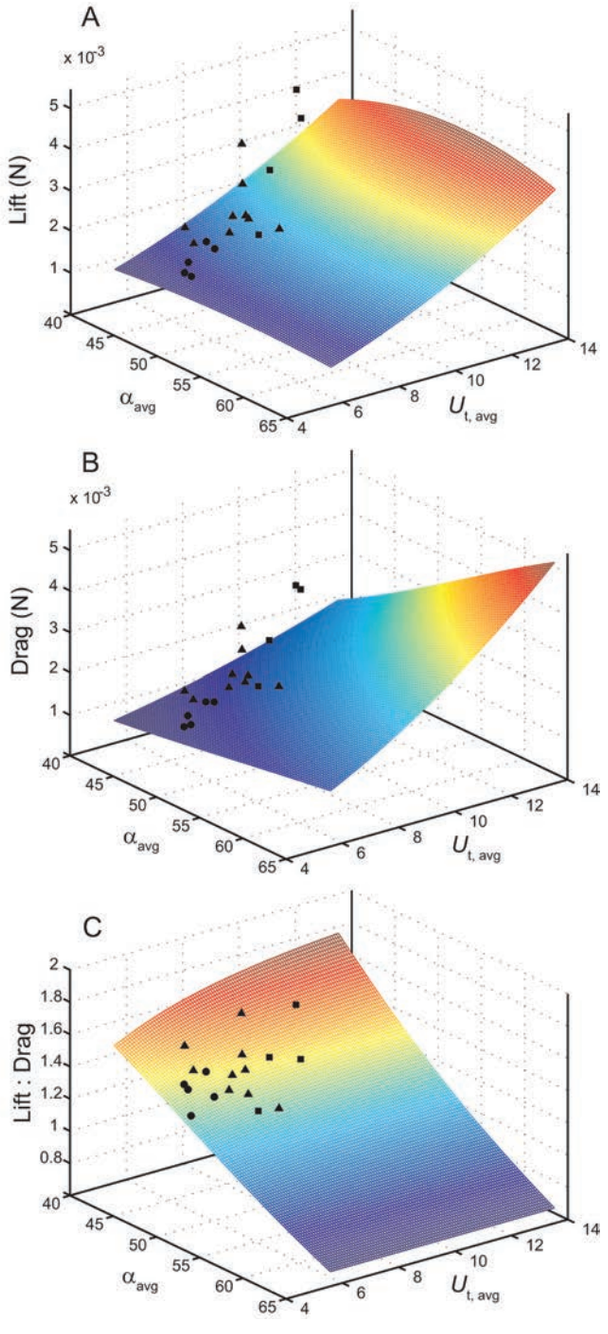

Figure 6. Stroke-averaged aerodynamic lift (*A*), drag (*B*), and lift-to-drag ratio (*C*) resulting from variation in mean wing tip velocity ($U_{t,avg}$) and stroke-averaged geometric angle of attack (α_{avg}). For individual bees, lift, drag, and lift-to-drag ratio during hovering (circles) and ascending (triangles) in air and hovering in heliox (squares) are plotted along the kinematic continuum of the aerodynamic model. Bees employed lesser α_{avg} than where maximum lift was estimated to occur (α_{avg} = 54.5°–56°), suggesting that bees' kinematic patterns do not maximize lift production but economize for lift-to-drag ratio.

while maintaining constant wing tip velocity. Although our aerodynamic model suggests that modulating only geometric angle of attack across the full 25° range evaluated could meet the lift requirements to support the modest pollen loads observed by Feurerbacher et al. (2003), bees in our study did not exhibit this strategy. Although outside of the scope of our aerodynamic model, variation in the phase of maximum wing rotation velocity relative to the stroke reversals, if advanced and sustained, could enhance force production via wing rotation (Sane 2003). However, it may also be possible that bees employed subtle changes in stroke amplitude that could not be calculated from images of blurred wing motion by Feurerbacher et al. (2003).

We limited our aerodynamic model to evaluate kinematic variability under conditions that approximate air. The stroke amplitudes observed during hovering in heliox are comparable to those observed during maximal load lifting in air in other bee species (Dillon and Dudley 2004; Buchwald and Dudley 2010). So, although our model does not estimate the resulting aerodynamic forces for hovering in heliox, the heliox kinematics could be reasonably expected under near-maximal load-lifting conditions in air and provide a kinematic continuum over which to evaluate strategies bees use to augment aerodynamic output. When heliox kinematics were modeled using a gas density parameter equivalent to heliox, aerodynamic forces were approximately 81% of those estimated from bees hovering in air. The source of this discrepancy, however, is not known. Our aerodynamic model calculates only lift due to wing translation and ignores other unsteady aerodynamic mechanisms, such as wing rotation, wing wake, and wing-wing interactions, though we would expect the relative contribution of these mechanisms to decrease, with respect to translational lift, as wing stroke amplitude increases (Altshuler et al. 2005). It is also possible that bees hovering in heliox were lighter than those hovering in air at the time of recording, as multiple bees were inside the flight chamber during any given flight condition and bees were free to consume sucrose water or collect pollen ad lib. Likewise, complete perfusion of the flight chamber with the heliox gas may not have occurred in some trials; for example, modeling the heliox aerodynamics with a gas density that instead represents 80% heliox (0.57 kg m^{-3}) produces aerodynamic forces similar to hovering in air. Thus, any one of these factors, or a combination of all three, may have contributed to the discrepancy in the lift estimated when using a density parameter equivalent to heliox.

Honeybees use high-frequency, low-amplitude wing strokes during hovering in air, in contrast with insects that use low-frequency, high-amplitude strokes such as *Drosophila*. Bees' ecologically relevant behaviors require that they carry pollen and nectar loads. Moreover, these aerodynamic challenges are compounded for honeybee populations and species from high-altitude habitats with low atmospheric densities (Underwood 1990; Hepburn et al. 1998). A substantial reserve capacity is necessary for successful flight under such conditions, yet despite complex wing kinematics, bees accommodate the

aerodynamic challenges of ascending flight and flight in hypodense atmospheres by simply increasing stroke amplitude and wing tip velocity while maintaining wingbeat frequency and the time course of geometric angle of attack. Other animals that meet the aerodynamic challenges of vertical flight primarily by controlling wing tip velocity (Dudley 1995; Chai et al. 1997; Lehmann and Dickinson 1997; Altshuler and Dudley 2003, 2004; Lehmann 2004; Altshuler et al. 2005; Vance et al. 2009) would likewise benefit from maintaining patterns of geometric angle of attack, as any modest increase in lift resulting from increased geometric angle of attack will be accompanied by a disproportionate increase in drag and reduction in efficiency. Bees reduce the control of aerodynamic output to simply manipulating stroke amplitude, which suggests that studies utilizing single camera views and/or low temporal resolution (Dudley 1995; Roberts et al. 2004; Vance et al. 2009) are capturing the most aerodynamically relevant features. However, further work is required to determine the aerodynamic consequences of the more subtle kinematic patterns we observed, including the phasing of wing rotation and clap and fling, especially under variable Re conditions, as well as mechanisms unresolved from the Feuerbacher et al. (2003) study. Insects limit the degrees of freedom by which they modulate aerodynamic performance, and manipulating a single kinematic parameter, such as stroke amplitude, can sufficiently and economically facilitate a broad range of vertical flight performance. However, constraints at the interface of aerodynamics and thermoregulation may ultimately require kinematic strategies that sacrifice aerodynamic efficiency for the heat production necessary for muscle function.

Acknowledgments

We thank David Shelton for the loan of equipment during filming and Nicholas Kostreski and J. Sean Humbert (University of Maryland, Department of Aerospace Engineering) for constructing the three-dimensional honeybee model and simulation videos used for the analysis of digitizing error. Funding was provided by a Nevada NASA Space Grant Fellowship (to J.T.V.), National Institutes of Health Fellowship F32 NS46221 (to D.L.A.), Office of Naval Research grant N00014-03-1-0604 (to M.H.D.), Packard Foundation grant 2001-17741A (to M.H.D.), and National Science Foundation grants IBN-0217229 (to M.H.D.) and IOS-0725030 (to S.P.R.).

APPENDIX A

Analysis of Digitizing Error

To assess the error associated with digitizing videos of insect flight, we compared the true kinematics of a three-dimensional (3D) digital model of a flying honeybee to the kinematics extracted using our digitizing methods. A 3D model of the honeybee was created using Matlab (Mathworks, Natick, MA) and Meshlab (open source; http://meshlab.sourceforge.net/), based on morphological measurements of the honeybee body and wings. The 3D model was projected into two dimensions for three simulated camera views (front, side, and top; fig. 1) using direct linear transformation (DLT) calibration parameters (DLT DataViewer; Hedrick 2008) obtained from a three-camera flight arena similar to that used in our study. The right and left wing motions of the 3D model were contralaterally symmetric and were programmed using Euler angles extracted from a video sequence of honeybee hovering flight (fig. B1, available online). The 3D model was prescribed a small degree of forward motion to ensure that digitizing body landmarks did not involve choosing static points but required the consistent digitizing of landmarks across the video sequence.

Using the image sequences from the three simulated camera views, we then performed calibration and digitizing according to the methods we describe in this study, based on the methods of Altshuler et al. (2005) and Fry et al. (2003). Our calibration assumed only the orthogonal arrangement of the three cameras and was naive to the actual DLT calibration parameters used to generate the three simulated camera views. Thus, our analysis estimates the combined calibration and digitizing error inherent with our methodology. The kinematic analysis of the flight sequence utilized six landmarks that were digitized using at least two camera views: head, tip of abdomen, left and right wing hinges, and left and right wing tips. To determine the angle of wing rotation (α), we superimposed a wire frame wing image over the model bee wing in all camera views and rotated the wire frame about the long axis (wing hinge to wing tip) until optimal overlap was achieved. From these landmarks, we determined the following kinematic variables during each frame of the recorded flight sequence: wing position angle (ϕ) within the stroke plane, wing deviation angle (θ) from the stroke plane, and geometric angle of attack (α). For each frame, digitizing error was calculated as the absolute difference between the digitized wing Euler angles and the true kinematics for each frame (fig. B1).

The mean digitizing error (mean $\pm$ SD) for six wingbeat cycles of the right and left wings was $2.8° \pm 2.0°$ for wing position angle (ϕ), $0.9° \pm 0.8°$ for wing deviation angle (θ), and $2.5° \pm 1.7°$ for geometric angle of attack (α). These results are similar to the sub-5° error in wing position and rotation angle associated with automated and manual digitizing methods reported by Ristroph et al. (2009). Similar to Ristroph et al. (2009), our analysis of digitizing error is limited to a 3D model of the insect with rigid, planar wings; however, honeybees demonstrate spanwise and chordwise wing deformation during flight (fig. 3). Mou et al. (2011) performed a comprehensive analysis of error using the same digitizing methods in our study, but they determined geometric angle of attack (α) by fitting the rigid-wing wire frame to a model wing image that incorporated spanwise and chordwise deformation image. Their analysis of error demonstrated wing position and deviation angle (ϕ and θ) less than 3° and geometric angle of attack (α) less than 4° of the true kinematics. Although we did not assess the potential error that may result from fitting a rigid-wing wire frame to a non-

rigid wing, our digitizing errors are comparable to those values reported by Ristroph et al. (2009) and Mou et al. (2011) when using similar digitizing methodologies (Fry et al. 2003).

Table A1: List of symbols

Symbol	Definition
AR	Advance ratio
n	Wingbeat frequency
L	Aerodynamic lift
D	Aerodynamic drag
$L:D$	Lift-to-drag ratio
Phase	Phase shift of maximum wing rotation velocity relative to the stroke reversal
U_{t}	Wing tip velocity
$U_{t,down}$	Maximum wing tip velocity during the downstroke
$U_{t,up}$	Maximum wing tip velocity during the upstroke
V_{vert}	Vertical velocity
α_{aero}	Aerodynamic angle of attack
α	Geometric angle of attack
α_{avg}	Stroke-averaged geometric angle of attack
α_{min}	Minimum geometric angle of attack (occurs near midstroke)
$\dot{\alpha}$	Wing rotation velocity
$\dot{\alpha}_{ventral}$	Maximum wing rotation velocity at the ventral stroke reversal
$\dot{\alpha}_{dorsal}$	Maximum wing rotation velocity at the dorsal stroke reversal
β	Stroke plane angle
β_{r}	Stroke plane angle relative to the body
θ	Wing deviation angle from the stroke plane
Θ	Amplitude of deviation from the stroke plane
ϕ	Wing position angle within the stroke plane
$\phi_{ventral}$	Maximum wing angle ventral to the wing hinge
ϕ_{dorsal}	Maximum wing angle dorsal to the wing hinge
Φ	Wing stroke amplitude
χ	Body angle
ω	Wing angular velocity

Literature Cited

Alexander D.E. 1986. Wind tunnel studies of turns by flying dragonflies. J Exp Biol 122:81–98.

Altshuler D.L., W.B. Dickson, J.T. Vance, S.P. Roberts, and M.H. Dickinson. 2005. Short-amplitude high-frequency wing strokes determine the aerodynamics of honeybee flight. Proc Natl Acad Sci USA 102:18213–18218.

Altshuler D.L. and R. Dudley. 2003. Kinematics of hovering hummingbird flight along simulated and natural elevational gradients. J Exp Biol 206:3139–3147.

———. 2004. The physiology and biomechanics of bird flight across elevations. Integr Comp Biol 44:515.

Altshuler D.L., R. Dudley, and C.P. Ellington. 2004. Aerodynamic forces of revolving hummingbird wings and wing models. J Zool 264:327–332.

Borrell B.J. and M.J. Medeiros. 2004. Thermal stability and muscle efficiency in hovering orchid bees (Apidae: Euglossini). J Exp Biol 207:2925–2933.

Buchwald R. and R. Dudley. 2010. Limits to vertical force and power production in bumblebees (Hymenoptera: *Bombus impatiens*). J Exp Biol 213:426–432.

Chai P. 1997. Hummingbird hovering energetics during moult of primary flight feathers. J Exp Biol 200:1527–1536.

Chai P., J.S.C. Chen, and R. Dudley. 1997. Transient hovering performance of hummingbirds under conditions of maximal loading. J Exp Biol 200:921–929.

Chai P. and R. Dudley. 1996. Limits to flight energetics of hummingbirds hovering in hypodense and hypoxic gas mixtures. J Exp Biol 199:2285–2295.

Coelho J. and J. Mitton. 1988. Oxygen consumption during hovering is associated with genetic variation of enzymes in honeybees. Funct Ecol 2:141–146.

Dickinson M.H. 1994. The effects of wing rotation on unsteady aerodynamic performance at low Reynolds numbers. J Exp Biol 192:179–206.

Dickinson M.H. and K.G. Götz. 1993. Unsteady aerodynamic performance of model wings at low Reynolds numbers. J Exp Biol 174:45–64.

Dickinson M.H., F.-O. Lehmann, and S.P. Sane. 1999. Wing rotation and the aerodynamic basis of insect flight. Science 284:1954–1960.

Dillon M.E. and R. Dudley. 2004. Allometry of maximum vertical force production during hovering flight of Neotropical orchid bees (Apidae: Euglossini). J Exp Biol 207:417–425.

———. 2014. Surpassing Mt. Everest: extreme flight performance of alpine bumble-bees. Biol Lett 10:20130922.

Dudley R. 1995. Extraordinary flight performance of orchid bees (Apidae, Euglossini) hovering in heliox (80% He/20% O_2). J Exp Biol 198:1065–1070.

Dudley R. and C.P. Ellington. 1990. Mechanics of forward flight in bumblebees. II. Quasi-steady lift and power requirements. J Exp Biol 148:53–88.

Ellington C.P. 1984*a*. The aerodynamics of hovering insect flight. III. Kinematics. Philos Trans R Soc B 305:41–78.

———. 1984*b*. The aerodynamics of hovering insect flight. IV. Aerodynamic mechanisms. Philos Trans R Soc B 305: 79–113.

———. 1984*c*. The aerodynamics of hovering insect flight. VI. Lift and power requirements. Philos Trans R Soc B 305:145–181.

———. 1999. The novel aerodynamics of insect flight: applications to micro-air vehicles. J Exp Biol 202:3439–3448.

Feuerbacher E., J.H. Fewell, S.P. Roberts, E.F. Smith, and J.F. Harrison. 2003. Effects of load type (pollen or nectar) and load mass on hovering metabolic rate and mechanical power output in the honeybee *Apis mellifera*. J Exp Biol 206:1855–1865.

Fry S.N., R. Sayaman, and M.H. Dickinson. 2003. The aerodynamics of free-flight maneuvers in *Drosophila*. Science 300:495–498.

Greenewalt C.H. 1962. Dimensional relationships for flying animals. Smithson Misc Coll 144:1–46.

Harrison J.F., J.H. Fewell, S.P. Roberts, and H.G. Hall. 1996. Achievement of thermal stability by varying metabolic heat production in flying honeybees. Science 274:88–90.

Harrison J.M. 1986. Caste-specific changes in honeybee flight capacity. Physiol Zool 59:175–187.

Hedrick T.L. 2008. Software techniques for two- and three-dimensional kinematic measurements of biological and biomimetic systems. Bioinspir Biomim 3:034001.

Hepburn H.R., C. Youthed, and P. Illgner. 1998. Production of aerodynamic power in mountain honeybees (*Apis mellifera*). Naturwissenschaften 85:389–390.

Kesel A.B. 2000. Aerodynamic characteristics of dragonfly wing sections compared with technical aerofoils. J Exp Biol 203:3125–3135.

Lehmann F.-O. 2004. The mechanisms of lift enhancement in insect flight. Naturwissenschaften 91:101–122.

Lehmann F.-O. and M.H. Dickinson. 1997. The changes in power requirements and muscle efficiency during elevated force production in the fruit fly *Drosophila melanogaster*. J Exp Biol 200:1133–1143.

Lehmann F.-O. and S. Pick. 2007. The aerodynamic benefit of wing-wing interaction depends on stroke trajectory in flapping insect wings. J Exp Biol 210:1362–1377.

Lehmann F.-O., S.P. Sane, and M. Dickinson. 2005. The aerodynamic effects of wing-wing interaction in flapping insect wings. J Exp Biol 208:3075–3092.

Ma K.Y., P. Chirarattananon, S.B. Fuller, and R.J. Wood. 2013. Controlled flight of a biologically inspired, insect-scale robot. Science 340:603–607.

Marden J.H., G.H. Fitzhugh, M. Girgenrath, M.R. Wolf, and S. Girgenrath. 2001. Alternative splicing, muscle contraction and intraspecific variation: associations between troponin T transcripts, Ca^{2+} sensitivity and the force and power output of dragonfly flight muscles during oscillatory contraction. J Exp Biol 204:3457–3470.

Miller L.A. and C.S. Peskin. 2005. A computational fluid dynamics of "clap and fling" in the smallest insects. J Exp Biol 208:195–212.

Mou X.L., Y.P. Liu, and M. Sun. 2011. Wing motion measurement and aerodynamics of hovering true hoverflies. J Exp Biol 214:2832–2844.

Ristroph L., A.J. Bergou, J. Guckenheimer, Z.J. Wang, and I. Cohen. 2011. Paddling mode of forward flight in insects. Phys Rev Lett 106:178103.

Ristroph L., A.J. Bergou, G. Ristroph, K. Coumes, G.J. Berman, J. Guckenheimer, Z.J. Wang, and I. Cohen. 2010. Discovering the flight autostabilizer of fruit flies by inducing aerial stumbles. Proc Natl Acad Sci USA 107:4820–4824.

Ristroph L., G.J., Berman, A.J., Bergou, Z.J. Wang, and I. Cohen. 2009. Automated hull reconstruction motion tracking (HRMT) applied to sideways maneuvers of free-flying insects. J Exp Biol 212:1324–1335.

Roberts S.P. 2005. Effects of flight behaviour on body temperature and kinematics during inter-male mate competition in the solitary desert bee *Centris pallida*. Physiol Entomol 30:151–157.

Roberts S.P. and J.F. Harrison. 1998. Mechanisms of thermoregulation in flying bees. Am Zool 38:492–502.

Roberts S.P., J.F. Harrison, and R. Dudley. 2004. Allometry of kinematics and energetics in carpenter bees (*Xylocopa varipuncta*) hovering in variable-density gases. J Exp Biol 207: 993–1004.

Sane S.P. 2003. The aerodynamics of insect flight. J Exp Biol 206:4191–4208.

Sane S.P. and M.H. Dickinson. 2002. The aerodynamic effects of wing rotation and a revised quasi-steady model of flapping flight. J Exp Biol 205:1087–1096.

Schippers M.P., R. Dukas, R.W. Smith, J. Wang, K. Smolen, and G.B. McClelland. 2006. Lifetime performance in foraging honeybees: behavior and physiology. J Exp Biol 209: 3828–3836.

Spangler H.G. and S.L. Buchmann. 1991. Effects of temperature on wingbeat frequency in the solitary bee *Centris caesalpiniae* (Anthophoridae, Hymenoptera). J Kans Entomol Soc 64:107–109.

Suarez R.K., C.A. Darveau, K.C. Welch, D.M. O'Brien, D.W. Roubik, and P.W. Hochachka. 2005. Energy metabolism in orchid bee flight muscles: carbohydrate fuels all. J Exp Biol 208:3573–3579.

Suarez R.K., J.R.B. Lighton, B. Joos, S.P. Roberts, and J.F. Harrison. 1996. Energy metabolism, enzymatic flux capacities, and metabolic flux rates in flying honeybees. Proc Natl Acad Sci USA 93:12616–12620.

Underwood B.A. 1990. Seasonal nesting cycle and migration patterns of the Himalayan honeybee, *Apis laboriosa*. Nat Geogr Res 6:276–290.

Unwin D.M. and S.A. Corbet. 1984. Wingbeat frequency, temperature and body size in bees and flies. Physiol Entomol 9:115–121.

Usherwood J.R. and C.P. Ellington. 2002. The aerodynamics of revolving wings. I. Model hawkmoth wings. J Exp Biol 205:1547–1564.

Vance J.T. 2009. Experimental and natural variation in hovering flight capacity in bees, Hymenoptera: Apidae. UNLV Theses Paper 26.

Vance J.T., I. Faruque, and J.S. Humbert. 2013. Kinematic strategies for mitigating gust perturbations in insects. Bioinspir Biomim 8:016004.

Vance J.T., J.B. Williams, M.M. Elekonich, and S.P. Roberts. 2009. The effects of age and behavioral development on the flight capacity of honeybee (*Apis mellifera*). J Exp Biol 212: 2604–2611.

Wakeling J.M. and C.P. Ellington. 1997*a*. Dragonfly flight. 2. Velocities, accelerations and kinematics of flapping flight. J Exp Biol 200:557–582.

———. 1997*b*. Dragonfly flight. 3. Lift and power requirements. J Exp Biol 200:583–600.

Withers P. 1981. The effects of ambient air pressure on oxygen consumption of resting and hovering honeybees. J Comp Physiol B 141:433–437.

Zdunich P., D. Bilyk, M. MacMaster, and D. Loewen. 2007. Development and testing of the *Mentor* flapping-wing micro air vehicle. J Aircraft 44:1701–1711.